Confining enzyme clusters in supramolecular nanoreactors enhances cofactor-dependent cascade for chiral alcohol synthesis

Yan-Qing Zhang
East China University of Science and Technology
Yufei Cao
Tsinghua University
Xiao-Yan Zhang
East China University of Science and Technology
Tao Wang
East China University of Science and Technology
Mario Roque Huanca Nina
East China University of Science and Technology
Tao-Tao Feng
East China University of Science and Technology
Li-Cheng Wang
Tsinghua University
Hui-Lei Yu
East China University of Science and Technology
Jianhe Xu
East China University of Science and Technology
Jun Ge
Tsinghua University https://orcid.org/0000-0001-5503-8899
Yunpeng Bai (ybai@ecust.edu.cn)
East China University of Science and Technology https://orcid.org/0000-0002-6973-581X

Article

Keywords: multienzyme assembly, enzymatic catalysis, cofactor recycling, confinement effects, asymmetric reduction

Posted Date: December 4th, 2020

DOI: https://doi.org/10.21203/rs.3.rs-100523/v1

Abstract

Enzymes in living organisms work efficiently in confined environments through spatial organization. Constituting a bio-cascade reaction in nano-confined space *in vitro* for the efficient synthesis of high-value chiral chemicals is challenging. Herein, we confined a cofactor-dependent cascade in bacteriophage P22 nanoparticles for the synthesis of chiral alcohols. Compared to free enzymes, this supramolecular ensemble, P22-SP-*Bm*GDH-*Ss*CR, exhibited enhanced catalytic efficiency up to 14.5-fold towards various ketones and improved stereoselectivity up to > 99% *ee* towards 8 substrates, and 10 chiral alcohols with > 96% *ee* were synthesized. The recycling efficiency of nicotinamide adenine dinucleotide phosphate (NADPH) was increased by 7.5-fold. We demonstrated that the enhancement in cofactor recycling originates from the higher local concentration of NADPH in the nanoparticles due to the proximity effect of enzymes and confinement of nanoparticles. The preparative synthesis of chiral alcohols showed that the consumption of NADPH can be reduced by one magnitude compared with the conventional free enzyme system.

Introduction

Multi-enzyme catalysis that can run a series of reactions has drawn increasing attentions for the production of high-value chemicals in the past decade[1-6]. In this approach, cofactor recycling is fundamentally essential to drive reactions towards the desired direction [4,7-11]. With respect to industrial biocatalysis, many enzyme processes rely on cofactors for their catalytic activity[7,12]. Therefore, expensive cofactors, such as NAD(P)H and ATP, also need to be regenerated and recycled many times to reduce the production cost [9, 12,14]. Thus, it is a significant benefit to design a system with highly efficient recycling of cofactors, which is also a major challenge for biocatalysis.

Cell-free cofactor recycling can be achieved by integrating an auxiliary enzyme which catalyzes a sacrificial and inexpensive substrate to regenerate cofactors. For example, NADPH can be recovered from NAD^+ using a glucose dehydrogenase and glucose[15-20]. Generally, the main and auxiliary enzymes are used as free enzymes in the reaction solution. The cofactors, NAD(P)H and $NAD(P)^+$, diffuse in bulk and exchange between enzymes for recycling. On contrary, living organisms have evolved unique features to maximize the efficiency of cofactor utilization by the spatial organization of biocatalytic cascades in confined cellular environments, which accelerates complex chemical reactions and regulates enzymatic activity of metabolic network[21-27]. Therefore, there has been considerable interest in creating artificial nanostructures that can control the assembly and co-localization of multiple enzymes for cascade reactions *in vitro*[22-24,28-38]. The ultimate goal is to develop an alternative to conventional free enzymes, which can increase reaction efficiency for commercial production processes. However, to our knowledge, two major challenges still remain: (1) to design a feasible system with high stereoselectivity and efficient cofactor recycling for the synthesis of chiral chemicals at preparative scale and (2) to understand how much the cofactor recycling can be improved by the confined enzymes compared with that in the free enzyme system.

Among numerous nanostructures, virus-like particles (VLPs) is particularly attractive because it can load various cargos in the nano-sized compartments through the self-assembly of its scaffold proteins (SPs) and coating proteins (CPs)[39-43]. In particular, the pioneering work of Patterson *et al* demonstrated that single and multiple enzymes can be encapsulated in P22 VLPs for enzyme-catalyzed reactions[41,42]. But constituting an enzymatic cascade in VLPs with cofactor recycling for the chiral chemical synthesis has not been achieved yet. In this study, we utilized single P22 VLPs as confined nanoreactors and developed an approach that allowed *Ss*CR (PDB: 5GMO) and *Bm*GDH (PDB: 1GCO) to be encapsulated successfully into the P22 capsids. *Ss*CR can convert various ketones to industrially relevant chiral alcohols[44], and *Bm*GDH has been widely used for NADPH recycling in biocatalysis. Distinguished from enzymes that clustered loosely without a defined boundary[31], herein, the double enzymes were confined tightly in nano-sized protein cages, enhancing the *in-situ* recycling of cofactors in nanoreactors (**Fig. 1a**). Among 12 tested ketones, 10 substrates were converted into chiral alcohols with >96% *ee*, and the stereoselectivity of the confined enzyme cluster (P22-SP-*Bm*GDH-*Ss*CR) towards 8 ketones was enhanced up to 99.9% compared to free enzymes. Moreover, P22-SP-*Bm*GDH-*Ss*CR accelerated the cofactor recycling of NADPH by up to 7.5-fold. We proved that the improvement of enzymatic reaction and cofactor recycling was caused by the higher local concentration of NADPH confined in the P22 nanoparticles through experiments and molecular simulation. The nanoconfined enzyme clusters was then used to synthesize 4 industrially important chiral alcohols at preparative scale, which significantly reduced the consumption of the expensive NADPH cofactor by one magnitude compared to the traditional free enzyme cascades.

Results And Discussion

Synthesis of enzyme-P22 nanoreactors

The single enzyme (monomeric *Ss*CR) encapsulated P22 nanoparticles (P22-SP-*Ss*CR, **Fig. 1b**) were synthesized by following a well-defined protocol (**Table S1**)[41]. Typically, the *Ss*CR gene (37.0 kDa) was ligated with the truncated SP gene (18.0 kDa), and then inserted into the CP-containing plasmid pRSFDuet-1 (**Fig. S1a**). Expression of the *Ss*CR-SP fusion proteins (**Fig. 1c**) and CPs in *E. coli* BL21(DE3) resulted in the self-assembly of P22-SP-*Ss*CR nanoparticles, which were separated by ultracentrifugation on a 35% (w/v) sucrose cushion (**Fig. S1b**) and purified by the size-exclusion chromatography (SEC) to remove other proteins (**Fig. S1c**). The *Ss*CR-SP fusion proteins and CPs migrated at approximately 55.0 kDa and 46.7 kDa in sodium dodecyl sulphate-polyacrylamide gel electrophoresis (SDS-PAGE), respectively (**Fig. 1d**). The P22-SP-*Ss*CR nanoparticles are spherical and monodispersed in negatively stained transmission electron microscopy (TEM, **Fig. 1e**) with an average size of 64.7 ± 0.4 nm determined by dynamic light scattering (DLS, **Fig. S1d**), larger than that of empty P22 (54.4 ± 1.9 nm)[41]. SEC coupled with multi-angle laser light scattering (SEC-MALS) showed a single peak of P22-SP-*Ss*CR, corresponding to the molecular weight (M_w) of 30.9 MDa (**Fig. S1e**). According to the M_w of P22 without SP (19.1 MDa), 214 enzymes were encapsulated into a single capsid, corresponding to a local concentration of 6.13 mM *Ss*CR. This number is slightly smaller than that in the study of Patterson et al. (~250 monomeric protein AdhD per capsid, 7.16 mM)[41], which attributes to the higher M_w of *Ss*CR (37.0

kD) compared to AdhD (32.0 kDa). It suggested that a soft oligopeptide linker between the enzyme and SP can improve protein folding inside particles[42]. Here, three nanoparticles with different oligopeptide chains, P22-SP-$(GGS)_3$-*Ss*CR, P22-SP- $GSAG_4TG_2A$-*Ss*CR and P22-SP-$(G_4S)_3$-*Ss*CR, were prepared and their specific activity (U/mg $_{enzyme}$) and gross activity (U/mg $_{particle}$) towards MBF (**1**) were tested (**Table S2**). P22-SP-$GSAG_4TG_2A$-*Ss*CR showed the highest activity of 10.16 ± 0.24 U/mg $_{enzyme}$ and 2.56 ± 0.06 U/mg $_{particle}$ among the three particles, and therefore this particle, still denoted P22-SP-*Ss*CR, was used in the following experiments.

Although multiple enzymes can be encapsulated in nanosized P22 particles[42], it remains a challenge to package large enzymes and maintain their activity because of the limited conformation flexibility[39]. Particularly, *Bm*GDH (115.1 kDa) is a tetramer and lacks the salt bridge that stabilizes the subunit interaction in the Q-interface. Thus, the complex of its four subunits is sensitive to the external environment change, leading to enzyme deactivation when encapsulated in the P22 capsid. To address this problem, 7 genetic circuits containing different gene combinations of *Bm*GDH, *Ss*CR and SP were designed and tested for their catalytic activity towards glucose (**Table S3**). The simple fusion of *Bm*GDH and SP (SP-*Bm*GDH) in circuit 1 and 2 did not generate active enzymes. Similarly, the direct fusion of *Ss*CR and *Bm*GDH with SP in circuit 3 and 4 were inactive towards glucose. We speculated that *Bm*GDH cannot form the correct quaternary structure because the chains of fusion protein were too rigid to get contact. To demonstrate this, an independent *Bm*GDH gene was inserted into circuit 5 without fusion with SP-*Ss*CR, and the generated nanoreactors displayed a weak activity of 80 U/g $_{enzyme}$ towards glucose. This result demonstrated that a few free *Bm*GDH subunits inside P22 capsids can form correct structures with the *Bm*GDH subunits in the fusion proteins. Then, we inserted an independent *Bm*GDH gene besides the original fused genes (SP-*Bm*GDH-*Ss*CR and SP-*Ss*CR-*Bm*GDH), which gave the circuit 6 and 7 respectively (**Table S3**). As a result, the as-synthesized P22-SP-*Bm*GDH-*Ss*CR (**Fig. 1f and g**) and P22-SP-*Ss*CR-*Bm*GDH displayed the activity of 500 and 600 U/g $_{enzyme}$ successfully.

The composition of P22-SP-*Bm*GDH-*Ss*CR was further analyzed. Three clear bands were observed in SDS-PAGE, corresponding to SP-*Bm*GDH-*Ss*CR (84.5 kDa), CP (46.6 kDa) and free subunits of *Bm*GDH (28.1 kDa) (**Fig. 1h**). The spherical particles have a larger average diameter of 72.4 ± 0.8 nm (**Fig. 1i**) and a higher M_w of 36.4 MDa compared with P22-SP-*Ss*CR (**Fig. S1g, h**). These results demonstrated that both *Ss*CR and *Bm*GDH were encapsulated into the P22 particles successfully. The densitometry analysis of SDS-PAGE indicates that 29 *Bm*GDH and 176 *Ss*CR were encapsulated in a capsid. The confined concentrations of *Bm*GDH and *Ss*CR in the nanoreactors are calculated as 0.89 and 5.0 mM, respectively.

Enzymatic kinetics for enzyme P22 nanoreactors

P22-SP-*Ss*CR displayed the highest activity at pH 6.0 and 30°C in a phosphate buffer saline solution, which is similar with SP-*Ss*CR (**Fig. S2a, b**), and its stability was improved when incubated at pH 5.07.0 (**Fig. S2c**). The reduction and oxidation activity towards MBF (**1a**) and glucose of P22-SP-*Bm*GDH-*Ss*CR and P22-SP-*Ss*CR-*Bm*GDH were determined respectively (**Table S4)**. The enzyme which was not linked to

SP directly exhibited higher activity, because it is more flexible than the enzyme that linked to SP. Considering the total activity of both *Ss*CR and *Bm*GDH, P22-SP-*Bm*GDH-*Ss*CR was selected for the following evaluation of catalytic property.

The kinetic constants (k_{cat}, K_M, and k_{cat}/K_M) of P22-SP-*Bm*GDH-*Ss*CR for the asymmetric reduction of four industrially useful substrates were compared with those of SP-*Ss*CR (**Table 1**). In general, all the data followed the Michaelis-Menten kinetics (**Fig. S3** and **Fig. S4**). P22-SP-*Bm*GDH-*Ss*CR exhibited 14.5-fold enhancement in catalytic efficiency (k_{cat}/K_m) for MBF (**1a**) compared with the free enzyme SP-*Ss*CR, which was contributed by 7-fold decrease in K_m and 2-fold increase in k_{cat}, respectively. The enhancement in catalytic efficiency was also observed for **1b** (8.2-fold) and **1c** (1.2-fold), but decreased by 10-fold for **1d**. Thus, whether the confinement effect can increase reaction efficiency for *in vitro* biocatalysis is substrate-dependent, which is in agreement with the recent studies[38,39,45,46.] The k_{cat}/K_m values of $NADP^+$ and glucose were 345 and 2.5 $s^{-1}mM^{-1}$, respectively (**Table S5**). For NADPH, the k_{cat}/K_m is 1249 $s^{-1}mM^{-1}$ which is higher than $NADP^+$ due to the higher reductive activity of *Ss*CR.

The improved NADPH recycling efficiency in P22-SP-*Bm*GDH-*Ss*CR

The time-course conversions of **1a** by free enzymes and P22-SP-*Bm*GDH-*Ss*CR were performed for the measurement of NADPH recycling efficiency (**Fig. 2**). In the free enzyme system, free *Bm*GDH was added to recover NADPH (**Fig. 2a**). In contrast, P22-SP-*Bm*GDH-*Ss*CR can catalyze the reaction self-sufficiently without the addition of free *Bm*GDH (**Fig. 2b**). In this case, NADPH was recycled *in situ* between *Ss*CR and *Bm*GDH which were co-confined in proximity inside P22 nanoparticles. It is hypothesized that the proximity of double enzymes in the confined nanoreactor can shorten the diffusion distance of NADPH and $NADP^+$, which may enhance the NADPH recycle efficiency as it is unstable and consumed by other oxidants during reaction.

First, only a small amount of $NADP^+$ (0.1 mM) was employed (**Fig. 2c**, squares), which was 50-fold lower than MBF concentration (5 mM). The complete conversion of MBF relied on the life of NADPH and its recycling times. The averaged NADPH recycles (the ratio of the concentration of converted substrates to the concentration of NADPH) represents the recycling efficiency. To compare the performance of different catalysts, the same activity of *Bm*GDH (0.28 U) was doped with SP-*Ss*CR and P22-SP-*Bm*GDH-*Ss*CR nanoreactors because the oxidization of glucose was the rate-limiting step. 100% conversion was achieved for the reaction catalyzed by P22-SP-*Bm*GDH-*Ss*CR at approximately 12 h (**Fig. 2c**, red squares), corresponding to averaged 50 NADPH recycles. This suggests that P22-SP-*Bm*GDH-*Ss*CR is self-sufficient to complete the reaction without external *Bm*GDH. Notably, the reaction catalyzed by SP-*Ss*CR was slower, with only 77.6% substrate was converted after 24 h (**Fig. 2c**, blue squares). The faster conversion in P22-SP-*Bm*GDH-*Ss*CR system represents the advantage of the *in situ* NADPH recycling between *Ss*CR and *Bm*GDH that were co-confined in proximity in P22 nanoparticles.

To further compare the NADPH recycling efficiency, we repeated the reactions under the same conditions while reducing the concentrations of NADPH (**Fig. 2c**, circles and triangles). When $NADP^+$ dropped to 10

μM, 100% conversion was still obtained after 12 h corresponding to averaged 500 NADPH recycles for P22-SP-*Bm*GDH-*Ss*CR (**Fig. 2c**, red circles). At 1 μM, the reaction rate significantly decreased, however, nearly 60% conversion was obtained at 24 h, corresponding to nearly 3000 NADPH recycles even at such low concentration of $NADP^+$ (**Fig. 2c**, red triangles). Considering that the concentration of $NADP^+$ was decreased by 100-fold (from 100 to 1 μM), the conversion decreased only from 100% to 60%, demonstrating that the reaction inside the P22-SP-*Bm*GDH-*Ss*CR nanoparticles is more "robust" to the NADPH change. In contrast, the reaction rates catalyzed by SP-*Ss*CR decreased more rapidly with the change of $NADP^+$ at each concentration of $NADP^+$. At 1 μM $NADP^+$, only 8% conversion was achieved at 24 h, corresponding to 400 NADPH recycles, which was 7.5-fold lower than that of P22-SP-*Bm*GDH-*Ss*CR (3000 recycles). In conclusion, we found that the co-clustering of double enzymes inside the nano-sized P22 particles can effectively enhance the recycling efficiency of the key intermediate NADPH especially at the low concentrations of NADPH.

Improved efficiency revealed by coarse-grained molecular simulations

There are several theories to explain why spatial organization of enzymes improves reaction efficiency[38]. The prevailing one is that the close proximity between enzymes prevents loss of reaction intermediates, such as NADP(H), by diffusion and favors substrate channeling[27,31]. Someone think that colocalization (or confinement) facilitates a local increase in reagent concentration, which increases the probability of events leading to reactions[47,48]. Here, we hypothesized that P22-SP-*Bm*GDH-*Ss*CR not only positions the double enzymes in close proximity, but also confines the reaction inside the nanoparticles, thus leading to a higher local concentration of NADPH. Coarse-grained molecular simulation was used to demonstrate this hypothesis (**Fig. 3a)**. The substrate (S*) and NADPH (M) are converted to the product (P) and $NADP^+$ (S) by *Ss*CR (E_1). $NADP^+$ (S) was then converted to NADPH (M) by *Bm*GDH (E_2), which was unstable and decayed to $NADP^+$ (S) with a certain probability. As shown in **Fig. 3b**, the "cluster" reaction model containing 50 enzyme molecules was confined in a cubic box of 40×40×40 (σ), simulating the double enzyme nanoreactor with a E_1 to E_2 ratio of 1:1. As control group, a free enzyme model, named "*homo*", contained enzymes which distributed and moved freely without clustering (**Fig. 3c**). The concentration of NADPH at the beginning is described by $c_M = N_M / N$, where N_M is the number of NADPH (M) molecules and N is the sum of NADPH and water molecules. The activity of E_1 and E_2 in the cluster equals to that in the homo model.

The time-course reaction simulation suggested that both the reaction rates of "cluster" and "homo" increased with higher concentration of NADPH (**Fig. S5**), correlating well with the above observations in **Fig. 2**. In particular, reactions proceeded faster in the enzyme "cluster" model. Reaction rates against different substrate concentrations of NADPH were showed in **Fig. 3d**. At every concentration, the enzyme cluster showed a higher reaction rate than the free enzyme. The ratio of the two reaction rates was calculated (**Fig. 3d, inset**), and the difference was more significant at lower concentrations of NADPH, which also agreed well with the experimental results (**Fig. 2**). By simulation, we discovered the differences of reaction rates were caused by the distribution of NADPH molecules (**Fig. 3e**) in the two reaction

systems. In the homo model, NADPH distributed uniformly in the space without accumulation and the concentrations were nearly the same at different spaces. In contrast, a higher density of NADPH was observed in the cluster region as indicated by the light blue area. In this region, the plot showed an apparent peak whereas the concentration dramatically decreases outside the region, indicating that the NADPH molecules were accumulated and confined in the P22 cluster.

To verify the simulation, we performed the asymmetric reduction of MBF by P22-SP-*Bm*GDH-*Ss*CR in the presence of a NADPH fluorescent probe TCF-MQ. TCF-MQ is a small and sensitive probe to monitor NADPH, but did not respond to $NADP^+$ (**Fig. S6**)[49]. The negative control which contained the purified P22-SP-*Bm*GDH-*Ss*CR, 10 μM TCF-MQ, and 100 μM $NADP^+$ did not show any fluorescence (**Fig. S7a**). In contrast, the positive control containing 100 μM NADPH showed the fluorescence which evenly distributed throughout the space under the same condition (**Fig. S7b**). Next, we started the reaction by adding 5 mM MBF and 10 mM glucose into the negative sample, which was observed using a confocal fluorescence microscope after 10 min (**Fig. S7c, d**). Clearly, fluorescent dots were found using the maximum magnification (100×, 1 μm scale), indicating the generation of NADPH due to the coupled reaction. More importantly, the fluorescence was confined inside the P22-SP-*Bm*GDH-*Ss*CR nanoparticles, which was different from the positive control. This result demonstrated that the concentration of NADPH in the nanoreactor was higher than that in the free enzyme solution, which was in agreement with the simulation. Thus, P22-SP-*Bm*GDH-*Ss*CR can recover and maintain more intermediates (NADPH) inside the P22 nanoparticles through the physical proximity and confinement of the double enzymes, which promotes the high recycling efficiency of NADPH for a faster reaction in the enzyme cluster.

Asymmetry synthesis of chiral alcohols by P22-SP-*Bm*GDH-*Ss*CR nanoreactor

With P22-SP-*Bm*GDH-*Ss*CR in hand, we evaluated its capacity for the asymmetric synthesis of 12 chiral benzylic alcohols without adding external *Bm*GDH (**Fig. 4**). Structurally diverse substrates were reduced successfully with analytical yields of 99%, affording 10 chiral alcohols with high optical purity (**2a**-**2m**, from 96% to >99% *ee*) except **2i** (89% *ee*) and **2j** (71% *ee*). Notably, the stereoselectivity of P22-SP-*Bm*GDH-*Ss*CR towards 8 substrates (**2e**, **2f**, **2g**, **2h**, **2k**, **2l**, >99% *ee*; **2i**, 89% *ee*; **2j**, 71% *ee*) was enhanced significantly compared with that of free *Ss*CR (73%, 87%, 90%, 80%, 88%, 86%, 72% and 37% *ee*, respectively). Besides, the high stereoselectivity of *Ss*CR towards **2a**, **2b**, **2d** and **2m** were maintained by P22-SP-*Bm*GDH-*Ss*CR (96%99% *ee*). In previous studies, the precise control over the stereoselectivity of ketoreductases is a major challenge, and time-consumed protein evolution is usually needed to acquire the desired stereopreferences[50]. In contrast, we showed that encapsulation of a ketoreductase in P22 nanoparticles can enhance its stereoselectivity without directed evolution, which, to our knowledge, has not been reported before. This could be explained by the increase in the difference of activation energy between the favorable and unfavorable transition states of enzyme-substrate complex due to confinement. However, to date it still faces notable challenges to demonstrate through calculation due to the lack of high-resolution internal structures of confined enzymes.

To demonstrate the potential of P22-*Bm*GDH-*Ss*CR for industrial biocatalysis, we scaled up the reaction for the synthesis of **2a**, **2d**, **2l** and **2m**. Initially, 50 mM substrates (**2a** or **2m**) and 0.5 mM $NADP^+$ were catalyzed by the extract of *E.coli*/P22-*Bm*GDH-*Ss*CR in a 50 mL reaction system at 25°C (**Fig. 4**, entry 1 and 2). After 5 h, 96% and 86% yields were achieved for **2m** and **2a** after column chromatography, respectively. Next, the amount of $NADP^+$ was further reduced by one magnitude to 0.05 mM for **2a** in a 100 mL system (entry 3). Surprisingly, the reaction also finished within 5 h at such low cofactor concentration with a lower catalyst loading (44 mg L^{-1}), while the conversion, yield and space-time yield (STY) were similar with the above. Inspired by this result, **2d** and **2l** were further synthesized at 0.05 mM $NADP^+$ with 36 mg L^{-1} enzymes. The reactions completed with 87% and 94% yields within 3.5 and 3 h, corresponding to 77 and 90 g L^{-1} d^{-1} STY, respectively (entry 4 and 5). All products with high *ee*, correlating well with the analytical preparation. For industrial biocatalysis, an appropriate amount of $NADP^+$ (~1% substrate concentration) is usually added to drive the reaction forward for high conversion and yield. With the increasing of substrate loading, the large consumption of the pricy $NADP^+$ is unavoidable. Here, we showed that the dosage of reductive cofactors can be reduced one magnitude to 0.1% of substrate concentration by P22-SP-*Bm*GDH-*Ss*CR without other cost while keeping the same and even higher productivity. With directed evolution, the activity of *Bm*GDH in the particles can be further improved, which displayed its advantage for efficient synthesis of important chiral alcohols for industrial biocatalysis.

Conclusion

In summary, we developed an approach to confine an enzyme cascade in P22 protein cages which improved cofactor *in-situ* recycling efficiency for asymmetric synthesis of chiral alcohols up to 7.5-fold compared with the free enzyme system. Molecular simulation and experiments demonstrated that the improvement of cofactor recycling was caused by the high local concentration inside P22 particles through the cooperation of double enzymes in proximity. An impressive catalytic feature is that the stereoselectivity of and the kinetic efficiency of confined enzyme towards 9 and 3 substrates were significantly enhanced compared to free enzyme, respectively. The scale-up synthesis demonstrated that the confined cascade can reduce the use of cofactors for industrial applications. The systematic study of the physical effect of nanoreactors on the stereoselectivity, activity and cofactor recycling efficiency of confined enzymes in this work provides insights into exploring the mechanism of natural enzyme clusters, inspiring new *in vitro* biocatalytic systems.

Declarations

Acknowledgements

This work was financially sponsored by the National Key Research and Development Program of China (Nos.2016YFA0204300, 2019YFA09005000 and 2018YFC1706200), the National Natural Science Foundation of China (Nos. 22078096, 21536004 and 21871085), the Key Project of the Shanghai Science

and Technology Committee (18DZ1112703) and the Natural Science Foundation of Shanghai (18ZR1409900).

References

1. Bornscheuer, U., Huisman, G., Kazlauskas, R. *et al.*Engineering the third wave of biocatalysis. *Nature* **485,** 185–194 (2012).
2. Schrittwieser, J. H., Velikogne, S., Hall, M. & Kroutil, W. Artificial biocatalytic linear cascades for preparation of organic molecules. *Rev.***118**, 270–348 (2018).
3. Sperl, J. M. & Sieber, V. Multienzyme cascade reactionsstatus and recent advances. *ACS Catal.* **8**, 2385-2396 (2018).
4. Valliere, M. A., Korman, T. P., Arbing, M. A. *et al.*A bio-inspired cell-free system for cannabinoid production from inexpensive inputs. *Chem. Biol.* (2020). https://doi.org/10.1038/s41589-020-0631-9
5. Mutti, F. G., Knaus, T., Scrutton, N. S., Breuer, M. & Turner, N. J. Conversion of alcohols to enantiopure amines through dual-enzyme hydrogen-borrowing cascades. *Science* **349**, 1525-1529 (2015).
6. Huffman, M. A., Fryszkowska, A., Alvizo, O. *et al.* Design of an in vitro biocatalytic cascade for the manufacture of islatravir. *Science* **366**, 1255-1259 (2019).
7. Zhao, H. & van der Donk, W. A. Regeneration of cofactors for use in biocatalysis. *Opin. Biotechnol.* **14**, 583-589 (2003).
8. Prier, C. K. & Arnold, F. H. Chemomimetic biocatalysis: exploiting the synthetic potential of cofactor-dependent enzymes to creat new catalysts. *Am. Chem. Soc.* **137,** 13992-14006 (2015).
9. Bowie, J. U., Sherkhanov, S., Korman, T. P. *et al.* Synthetic biochemistry: the bio-inspired cell-free approach to commodity chemical production. *Trends in Biotechnol.* **38**, 766-778 (2020).
10. Liao, C. S. & Seebeck, F. P. Asymmetric β-methylation of L- and D-α-amino acids by a self-contained enzyme cascade. *Chem. Int. Ed.* **59**, 7184-7187 (2000).
11. Andexer, J. N., & Richter, M. Emerging enzymes for ATP regeneration in biocatalytic processes. *ChemBioChem* **16**, 380-386 (2015).
12. Bergquist, P. L., Siddiqui, S. & Sunna, A. Cell-free biocatalysis for the production of platform chemicals. *Energy Res.* **8**, 193 (2020).
13. Wang, M., Chen, B. Q., Fang, Y. M. & Tan, T. W. Cofactor engineering for more efficient production of chemicals and biofuels. *Adv.* **35**, 1032-1039 (2017).
14. Schrittwieser, J. H., Sattler, J., Resch, V., Mutti, F. G. & Kroutil, W. Recent biocatalytic oxidation-reduction cascades. *Opin. Chem. Biol.* **15,** 249-256 (2011).
15. Wu, S. K., Snajdrova, R., Moore J. C., Baldenius, K. & Bornscheuer, U. T. Biocatalysis: enzymatic synthesis for industrial applications. *Chem. Int. Ed.* **59**, 2-34 (2020).
16. Ma, S. K., Gruber, J., Davis, C. *et al.* A green-by-design biocatalytic process for atorvastatin intermediate. *Green Chem.* **12**, 81-86 (2010).

17. Gong, X. M., Qin, Z., Li, F. L., Zeng, B. B., Zheng, G. W. & Xu, J. H. Development of an engineered ketoreductase with simultaneously improved thermostability and activity for making a bulky atorvastatin precursor. *ACS Catal.* **9,** 147-153 (2019).
18. Chen, M., Zhang, X.Y., Zhang, C. *et al.* Efficient stereoselective synthesis of structurally diverse γ-/δ-lactones using an engineered carbonyl reductase. *ChemCatChem* **11**, 2600-2606 (2019).
19. Chen, X., Zhang, H., Maria-Solano, M. A. *et al.* Efficient reductive desymmetrization of bulky 1,3-cyclodiketones enabled by structure-guided directed evolution of a carbonyl reductase. *Catal.* **2**, 931-941 (2019).
20. Schober, M., MacDermaid, C., Ollis, A. A. *et al.*Chiral synthesis of LSD1 inhibitor GSK2879552 enabled by directed evolution of an imine reductase. *Catal.* **2**, 909–915 (2019).
21. Agapakis, C., Boyle, P. & Silver, P. Natural strategies for the spatial optimization of metabolism in synthetic biology. *Chem. Biol.***8**, 527–535 (2012).
22. Vázquez-González, M., Wang, C. & Willner, I. Biocatalytic cascades operating on macromolecular scaffolds and in confined environments. *Catal.* **3**, 256-273 (2020).
23. Küchler, A., Yoshimoto, M., Luginbühl, S., Mavelli, F. & Walde, P. Enzymatic reactions in confined environments. *Nanotechnol.* **11**, 409-420 (2016).
24. Rabe, K. S., Müller, J., Skoupi, M. & Niemeyer, C. M. Cascades in compartments: en route to machine-assisted biotechnology. *Chem. Int. Ed.* **56**, 13574-13589 (2017).
25. Good, M. C., Zalatan, J. G. & Lim, W. A. Scaffold proteins: hubs for controlling the flow of cellular information. *Science* **332**, 680-686 (2011).
26. Savage, D. F., Afonso, B., Chen, A. H. & Silver, P. A. Spatially ordered dynamics of the bacterial carbon fixation machinery. *Science* **327**, 1258-1261 (2010).
27. Wheeldon, I., Minteer, S. D., Banta, S. *et al.* Substrate channeling as an approach to cascade reactions. *Chem.* **8**, 299-309 (2016).
28. Bugada, L. F., Smith, M. R. & Wen, F. Engineering spatially organized multienzyme assemblies for complex chemical transformation. *ACS Catal.* **8**, 7898-7906 (2018).
29. Shi, J. F., Wu, Y. Z., Zhang, S. H. *et al*. Bioinspired construction of multi-enzyme catalytic systems. *Soc. Rev.* **47**, 4295-4313 (2018).
30. An, S.G., Kumar, R., Sheets, E. D. & Benkovic, S. J. Reversible compartmentalization of de novo purine biosynthetic complexes in living cells. *Science* **320**, 103-106 (2008).
31. Castellana, M., Wilson, M. Z., Xu, Y. F. *et al.* Enzyme clustering accelerates processing of intermediates through metabolic channeling. *Biotechnol.* **32**, 1011-1018 (2014).
32. Zhang, G. Q., Quin, M. B. & Schmidt-Dannert, C. Self-assembling protein scaffold system for easy *in vitro* coimmobilization of biocatalytic cascade enzymes. *ACS Catal.* **8**, 5611-5620 (2018).
33. Brasch, M., Putri, R. M., de Ruiter, M. V. *et al.* Assembling enzymatic cascade pathways inside virus-based nanocages using dual-tasking nucleic acid tags. *Am. Chem. Soc.* **139**, 1512-1519 (2017).

34. Tsitkov, S. & Hess, H. Design principles for a compartmentalized enzyme cascade reaction. *ACS Catal.* **9**, 2432-2439 (2019).
35. Zhao, Z., Fu, J. L., Dhakal, S. *et al.* Nanocaged enzymes with enhanced catalytic activity and increased stability against protease digestion. *Commun.* **7**, 10619 (2016).
36. Ngo, T. A., Nakata, E., Saimura, M. & Morii, T. Spatially organized enzymes drive cofactor-coupled cascade reactions. *Am. Chem. Soc.* **138**, 3012-3021 (2016).
37. Chen, W. H., Vázquez-González, M., Zoabi, A., Abu-Reziq, R. & Willner, I. Biocatalytic cascades driven by enzymes encapsulated in metal–organic framework nanoparticles. *Catal.* **1**, 689–695 (2018).
38. Quin, M. B., Wallin, K. K., Zhang, G. & Schmidt-Dannert, C. Spatial organization of multi-enzyme biocatalytic cascades. *Biomol. Chem.* **15**, 4260-4271 (2017).
39. Aumiller Jr., W. M., Uchida, M. & Douglas, T. Protein cage assembly across multiple length scales. *Soc. Rev.* **47,** 3433-3469 (2018).
40. Tapia-Moreno, A., Juarez-Moreno, K., Gonzalez-Davis, O., Cadena-Nava, R. D. & Vazquez-Duhalt, R. Biocatalytic virus capsid as nanovehicle for enzymatic activation of Tamoxifen in tumor cells. *J.* **12**, 1600706 (2017).
41. Patterson, D. P., Prevelige, P. E. & Douglas, T. Nanoreactors by programmed enzyme encapsulation inside the capsid of the bacteriophage P22. *ACS Nano* **6**, 5000-5009 (2012).
42. Patterson, D. P., Schwarz, B., Waters, R. S., Gedeon, T. & Douglas, T. Encapsulation of an enzyme cascade within the bacteriophage P22 virus-like particle. *Chem. Biol.* **9**, 359-365 (2014).
43. Jordan, P., Patterson, D., Saboda, K. *et al.*Self-assembling biomolecular catalysts for hydrogen production. *Nature Chem* **8,** 179–185 (2016).
44. Shang, Y. P., Chen, Q., Kong, X. D., Zhang, Y. J., Xu, J. H. & Yu, H. L. Efficient synthesis of (*R*)-2-chloro-1-(2,4-dichlorophenyl) ethanol with a ketoreductase from *Scheffersomyces stipites* CBS 6045. *Synth. Catal.* **359**, 426-431 (2017).
45. Frey, R., Mantri, S., Rocca, M. & Hilvert, D. Bottom-up construction of a primordial carboxysome mimic. *Am. Chem. Soc.* **138**, 10072-10075 (2016).
46. Zhang, Y., Tsitkov, S. & Hess, H. Proximity does not contribute to activity enhancement in the glucose oxidase–horseradish peroxidase cascade. *Nat Commun***7,** 13982 (2016).
47. Grommet, A.B., Feller, M. & Klajn, R. Chemical reactivity under nanoconfinement. *Nanotechnol.***15,** 256–271 (2020).
48. Idan, O. & Hess, H. Origins of activity enhancement in enzyme cascades on scaffolds. *ACS Nano* **7**, 8658-8665 (2013).
49. Pan, X. H., Zhao, Y. H., Cheng, T. T. *et al.* Monitoring NAD(P)H by an ultrasensitive fluorescent probe to reveal reductive stress induced by natural antioxidants in HepG2 cells under hypoxia. *Sci.* **10**, 8179-8186 (2019).
50. Zhou, J. Y., Wang, Y., Xu, G. C. *et al.* Structural insight into enantioselective inversion of an alcohol dehydrogenase reveals a “polar gate” in stereorecognition of diaryl ketones. *Am. Chem. Soc.* **140**,

12645-12654 (2018).

Table

Table 1 | Kinetic parameters of asymmetric reduction of ketones by free and confined enzymes.

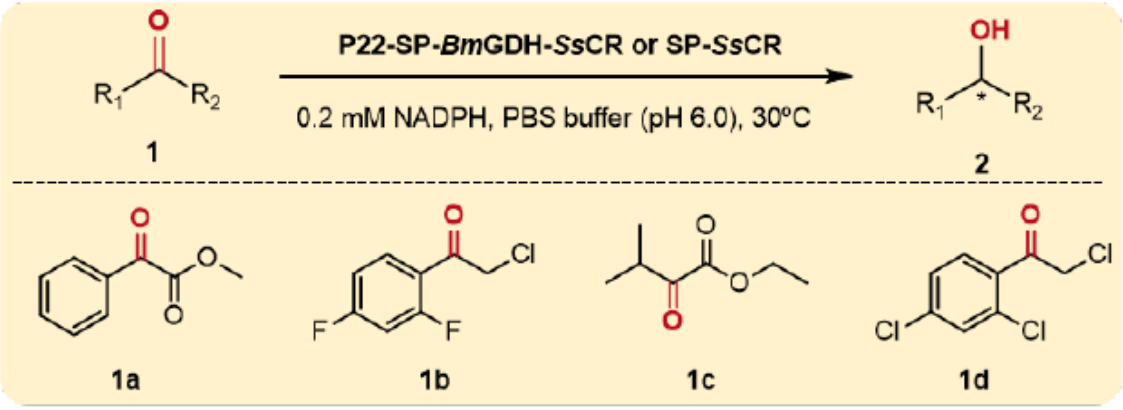

Substrate	SP-*Ss*CR[a]			P22-SP-*Bm*GDH-*Ss*CR[a]			Fold[b]
	K_M (μM)	k_{cat} (S^{-1})	k_{cat}/K_M (mM^{-1} S^{-1})	K_M (μM)	k_{cat} (S^{-1})	k_{cat}/K_M (mM^{-1} S^{-1})	
1a	206 ± 91	9.6 ± 0.4	46.4 ± 9.2	29.1 ± 8.4	20.2 ± 1.1	671 ± 54	14.5
1b	38.7 ± 11.3	3.2 ± 0.2	81.9 ± 6.9	30.5 ± 9.4	19.5 ± 0.9	672 ± 45	8.2
1c	104.8 ± 6.9	19.3 ± 0.3	185 ± 11	75.7 ± 11.7	16.6 ± 0.7	218 ± 31	1.2
1d	3.3 ± 0.5	8.9 ± 0.3	2794 ± 46	25.1 ± 5.6	10.0 ± 0.4	401 ± 20	0.1

[a]All enzymes were purified prior to characterization. The enzyme activity was determined in a pH 6.0, 100 mM sodium phosphate buffer, containing 0.2 mM NADPH in the presence of 0.01-2 mM substrates at 30°C. [b]Fold change in k_{cat}/K_M compared to SP-*Ss*CR. Substrates were methyl benzoylformate (**1a**), 2-chloro-2',4'-difluoroacetophenone (**1b**), ethyl 3-methyl-2-oxobutanoate (**1c**) and 2,2',4'-trichloroacetophenone (**1d**).

Figures

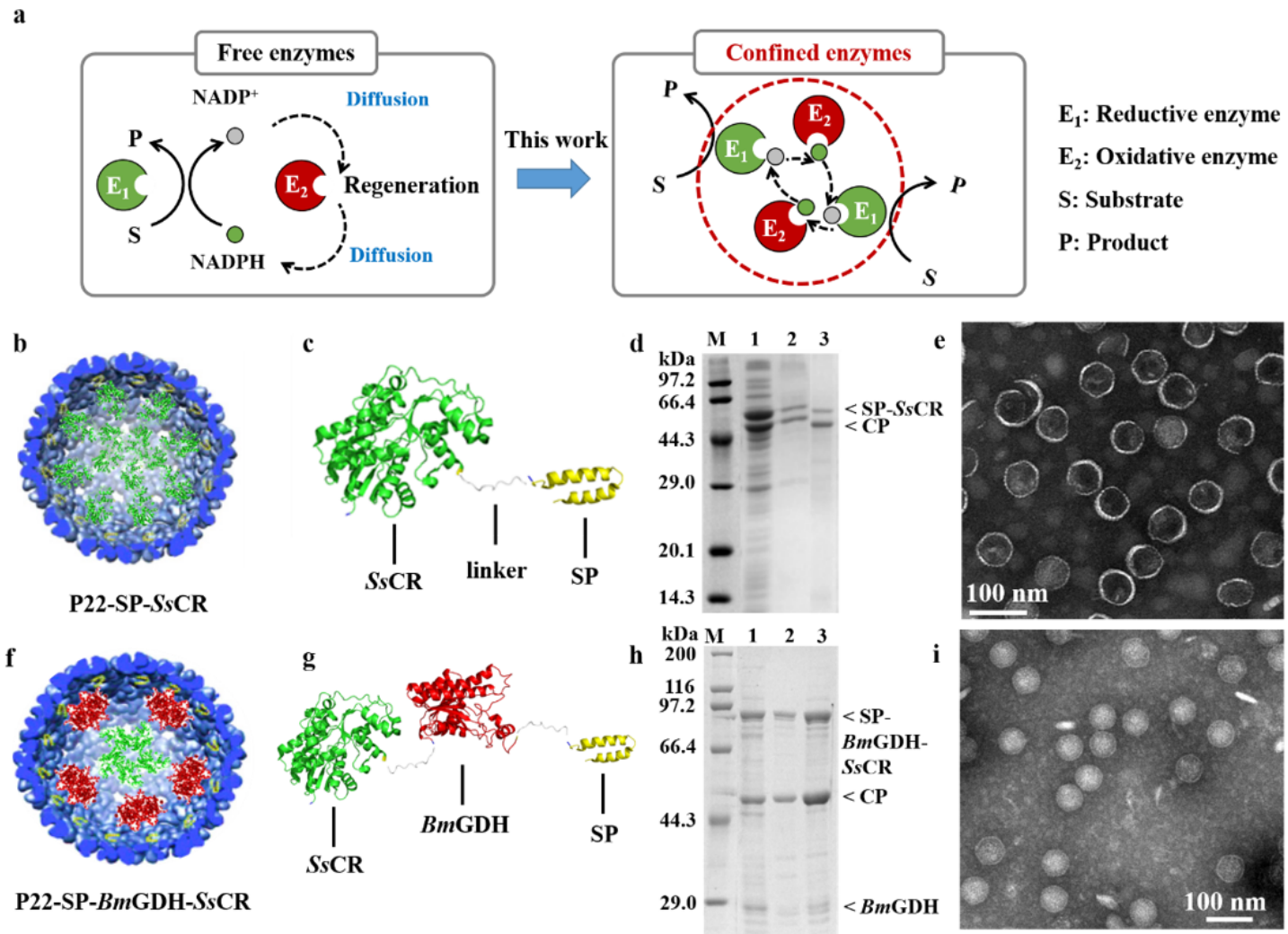

Figure 1

Preparation and characterization of single and double enzyme-P22 nanoreactors. a, schematic illustration of confined enzymes studied in this work. b and f, P22-SP-SsCR (b) and P22-SP-BmGDH-SsCR (f) nanoreactors. c and g, the fusion proteins of SP-SsCR (c) and SP-BmGDH-SsCR (g). d and h, the purified fusion proteins and CPs in P22-SP-SsCR (d) and P22-SP-BmGDH-SsCR (h) were analyzed by SDS-PAGE, respectively. e and i, the negatively stained TEM images of P22-SP-SsCR (e) and P22-SP-BmGDH-SsCR (i).

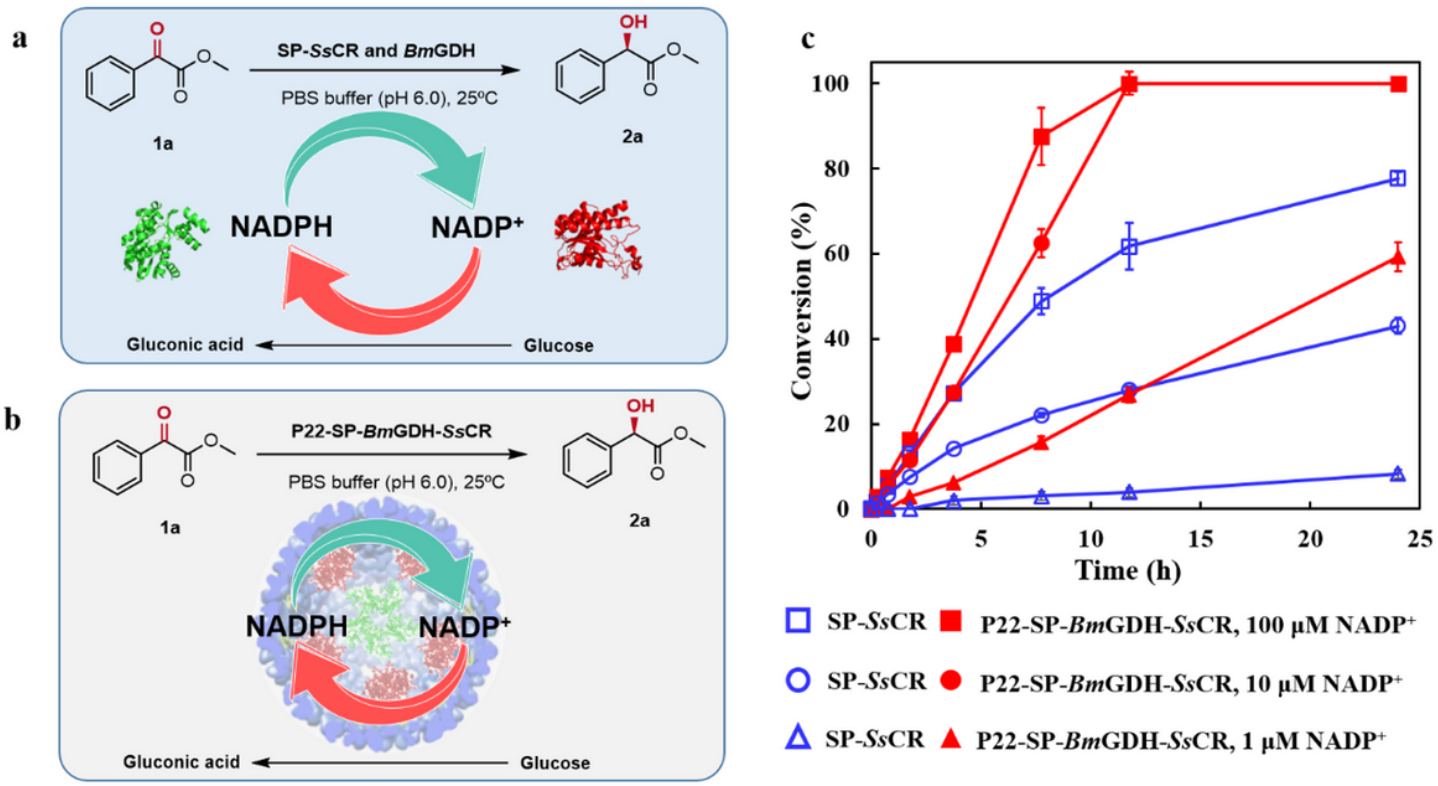

Figure 2

The time-course conversion of 1a by SP-SsCR and P22-SP-BmGDH-SsCR. The reactions were performed with (a) or without (b) the addition of free BmGDH for NADPH recycling. (c) Reaction condition for (a) and (b): [MBF]=5 mM, [NADP+]=0.1 mM, 10 μM and 1 μM respectively, [Glucose]=3.6 g/L, [BmGDH]=0.28 U (0.2 mg/L), [SP-SsCR]=13.5 mg/L (2.3 U), [P22-SP-BmGDH-SsCR]=66 mg/L (0.28 U for oxidation and 3.0 U for reduction), 100 mM PBS buffer, pH 6.0, 25°C.

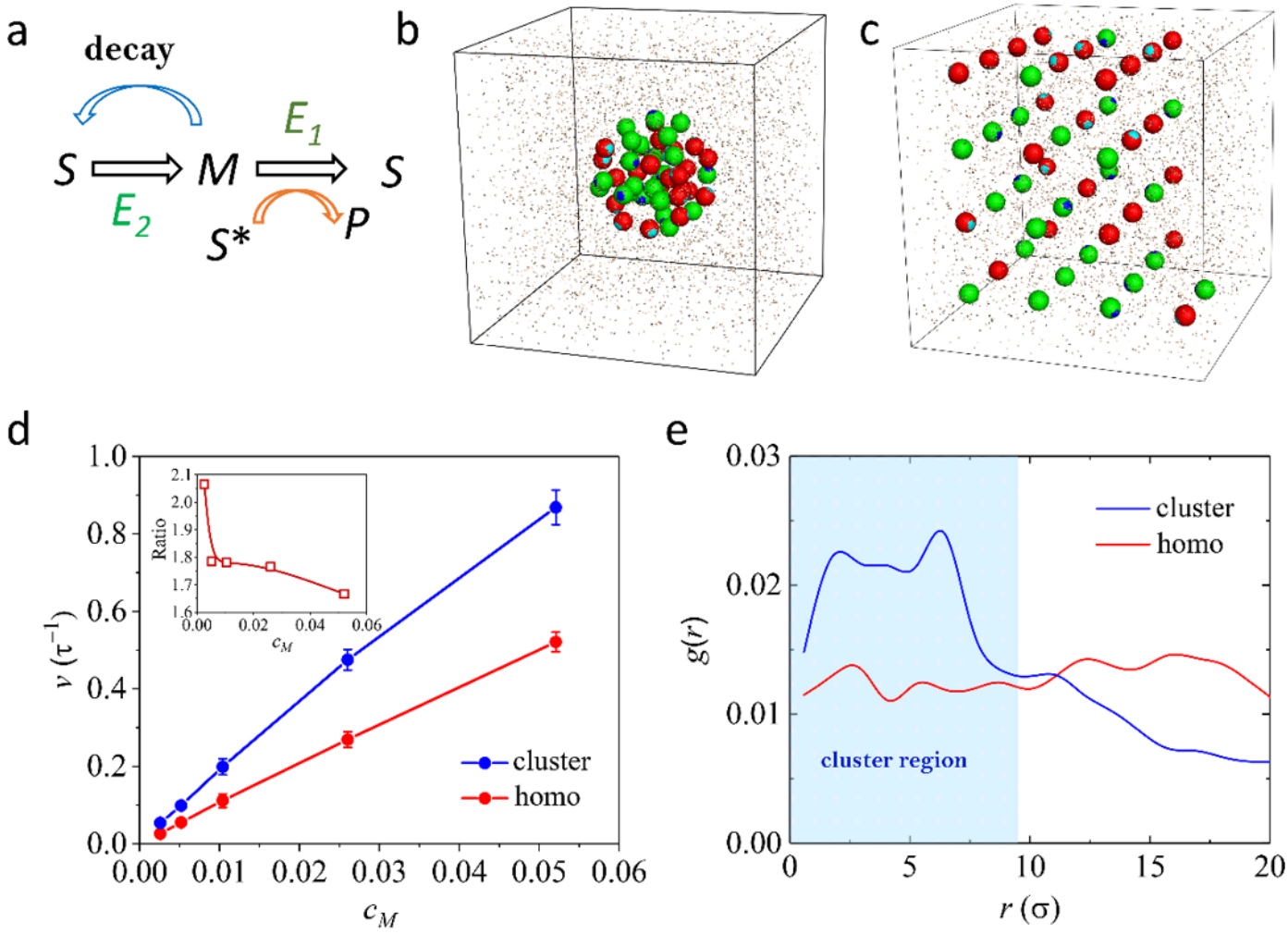

Figure 3

Simulation model and experimental results. (a) Cascade reaction pathway of enzyme clusters: E1 and E2 represent SsCR and BmGDH, respectively. NADP+ and NADPH were noted as S and M. S* is the substrate of E1, and P is the final product. NADPH is unstable, with a certain probability of decaying to NADP+. The relationship between the decay probability of M and time is shown in function: P=1-exp(-βt), where β indicates the rate of decay and β=1×10-7 τ -1. The ratio of turnover numbers of E1 to E2 was 4:1 b Enzymes are clustered in a 40×40×40 (σ) cubic box. (c) Two enzymes uniformly distribute in a 40×40×40 (σ) cubic box. (d) The reaction rate, v, was plotted against the NADPH concentrations. Inset: the ratio of the reaction rates of “cluster” and “homo” versus the NADPH concentrations. (e) Radial distribution function, g(r) of M. r is the distance between the position of NADPH molecular and the center of the box. g(r) was used to characterize the concentration distribution of M in the 40×40×40(σ) simulation box. Enrichment of intermediates can be observed in cluster region.

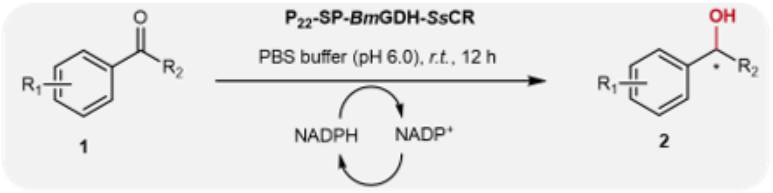

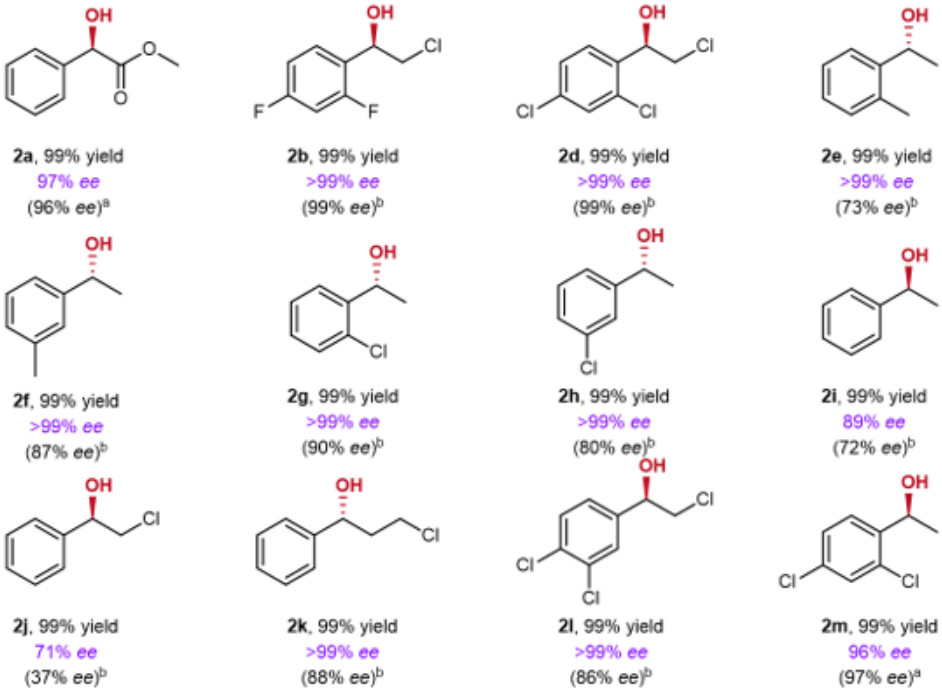

Preparative synthesis of various chiral alcohols by P22-SP-*Bm*GDH-*Ss*CR.

Entry	Product	Substrate (mM)	Catalyst (mg·mL^{-1})	NADP$^+$ (mM)	Time (h)	Conv. (%)	Yield (%)	STY (g·L^{-1}·d^{-1})	*ee* (%)
1[c]	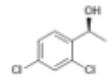	50	50	0.5	5	99.9	96	46	96
2[c]	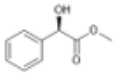	50	50	0.5	5	99.9	86	39	97
3[d]	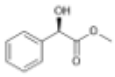	50	44	0.05	5	99.9	85	40	97
4[d]	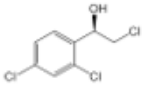	50	36	0.05	3.5	99.9	87	77	>99
5[d]	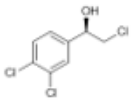	50	36	0.05	3	99.9	94	90	>99

Figure 4

Asymmetric synthesis of chiral benzylic alcohols by P22-SP-BmGDH-SsCR. Experiments were performed at milligram scale using E. coli crude extract containing P22-SP-BmGDH-SsCR resuspended in PBS buffer (pH 6.0), 5.0 mM substrate, 0.1 mM NADP+, 15 mM glucose at room temperature for 12 h. Yields were quantified by chiral GC based on the calibration curves of the corresponding reference products. aThe ee values of products generated by free enzyme SsCR were determined by chiral GC in this work. bThe ee

values of products generated by free enzyme SsCR in the parentheses were cited from ref 44. c,dReaction conditions: glucose (100 mM), cell extract of E.coli/P22-BmGDH-SsCR, 50c or 100d mL sodium phosphate buffer (100 mM, pH 6.0), 25 ℃.

Supplementary Files

This is a list of supplementary files associated with this preprint. Click to download.

- SI.docx